6) Fuels for fast neutron Generation IV reactors

Learning objectives

After you have completed the exercises in this chapter, you will be able to:

1) Assess the impact on fuel in-pile performance when introducing minor actinides
2) Assess the impact on fuel manufacture when introducing minor actinides
3) Assess the impact on fuel reprocessing when introducing minor actinides

Background:

The heart of a power reactor is its fuel. An enormous amount of heat produced in this component, which during its life is transmuted into hundreds of fission productions that affect its performance, as well as into other actinides. The integrity of the fuel is paramount for safety of the reactor, as it constitutes the first barrier for release of highly radioactive fission products into the environment. If the fuel melts or undergoes other phase transitions, it may have an impact both on reactor stability and on the integrity of the second barrier (the fuel cladding or coating). The integrity of the fuel cladding may also be challenged by chemical or mechanical interaction with the fuel, or by pressure resulting from release of gas produced by fission or alpha-decay of actinides.

Therefore, the design of a nuclear fuel for a power reactor must ensure that it remains sufficiently stable throughout its intended service-life. Neither should it constitute a threat to the integrity of the fuel cladding during nominal operation, nor during transients.

If we consider fuels for fast neutron Generation IV reactors, a particular aspect is that their chemical composition should allow for reprocessing of the spent fuel on an industrial scale. Moreover, the presence of americium and possibly curium in the fresh fuel requires modified fuel manufacturing methods and shielded fabrication facilities.

About half of the fast reactors that have been or are under operation relied on enriched uranium in either oxide or metallic form as fuel (see Table 1.1). In terms of the aforementioned requirements, there are advantages related to the use of uranium fuels, related to important features such as high temperature stability, thermal conductivity and fuel clad chemical interaction (FCCI). In general, the introduction of plutonium and minor actinides are detrimental for these properties.

In preceding chapters, the advantages of using so called high density fuels (metal alloys, nitrides and carbides) for the purpose of improving breeding have been shown in detail. In addition, these fuel compositions provide a considerably better thermal conductivity and hence an improved margin to failure during transients. Among their disadvantages are poorer stability at high temperature, higher fuel swelling rates, a less benign fuel-clad interaction, more complex fabrication methods and for metals alloy/carbide fuels, compatibility with industrially established reprocessing methods.

In the following sections, we provide basic thermo-physical and thermo-chemical data pertaining to each of these fuel options, in conjunction with empirical data for their performance under irradiation, when such are available. The connection between the basic properties and in-pile performance is discussed. Moreover, we highlight difficulties in fabrication resulting from the introduction of minor actinides and the corresponding poor high temperature stability of high density duels. Finally, possible issues related to reprocessing are commented on. The data sets here provided are limited to what is considered directly useful for pedagogical purposes. A more extensive treatment of Generation IV reactor fuels is found in the series ”Comprehensive Nuclear Materials”, published by Elsevier [Reference].

Thermal conductivity

The thermal conductivity of a fuel is one of its most important properties, and even more so in the context of Generation IV reactors. It directly determines the temperature difference between the surface and the centreline of the fuel. Thus, a higher thermal conductivity increases the margin to fuel melting or dissociation. It also reduces the rate of diffusion processes leading to gas release and chemical redistribution of fuel components.

The conductivity strongly depends on chemical form and decreases during irradiation. Actinide oxides have a very low thermal conductivity, mainly mediated by phonons (lattice vibrations). A large body of experimental data on UO_2 and $(U,Pu)O_2$ fuels have been acquired, indicating that for fully stoichiometric dioxides, there is little impact of plutonium concentration on the conductivity. However, since the oxygen potential of the Pu-O system is larger than for the U-O system, the thermodynamically stable compound tends to be sub-stoichiometric. In order to reduce the probability for internal cladding corrosion, MOX fuel therefore is produced with a certain degree of sub-stoichiometry, leading to a reduction in thermal conductivity.

Analysing experimental data and theoretical assessments, Carbajo recommends that the thermal conductivity λ of unirradiated $(U,Pu)O_{2-x}$ at 100% theoretical density (TD) be described by a sum of two terms representing phonon and electron conduction respectively [Ronchi 1999, Carbajo 2001]:

$$\lambda_{TD}(T,x) = 1.158\left(\frac{1}{A(x)+B(x)T} + 6400\left(\frac{1000}{T}\right)^{5/2}\exp\left(-\frac{16350}{T}\right)\right)$$

where A and B are functions of sub-stoichiometry x. The following expressions for A and B have been suggested to be valid in the temperature range $500\ K < T < T_{melt}$ [Duriez 2000]:

$$A(x) = 0.035 + 2.85x$$
$$B(x) = (0.286 - 0.715x)\times 10^{-3}$$

in units ensuring that all terms are expressed in Watts per meter and Kelvin. The above expression is displayed in Figure 6.1, where the impact of stoichiometry can be explored through the slider.

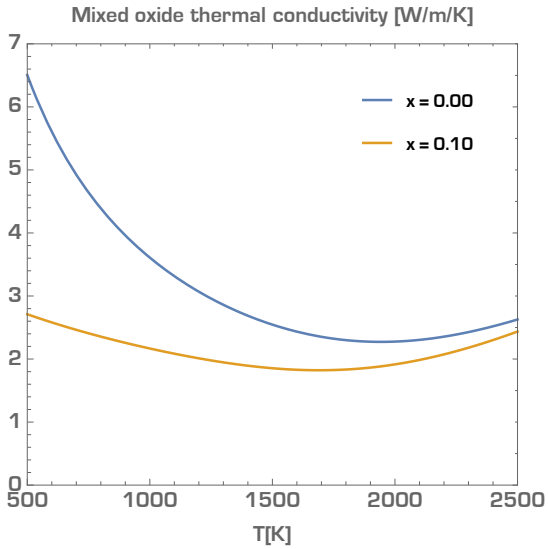

Figure 6.1: Thermal conductivity of 100% dense mixed oxide fuel [Carbajo 2001]

Measurements of the thermal conductivity of americium oxide [Bakker 1998, Nishi 2008], in conjunction with theoretical modelling of phonon conductivity [Lemehov 2003, Sobolev 2009], indicate that the major effect on thermal conductivity of americium introduction into MOX fuels derives from the concentration of oxygen

vacancies. The oxygen potential for the Am-O system is considerably larger than for Pu-O, which is reflected in the fact that americium oxides typically are fabricated with an O/M ratio of 1.9. We may therefore assume that the above given parametrisation of MOX conductivity can be applied to americium bearing fuels, as long as a proper account of the O/M ratio is undertaken.

Impact of porosity

The effective thermal conductivity is further reduced by the porosity P of the fuel. Oxide fuels are normally fabricated with 5-10% porosity to permit for swelling. The influence is strongly dependent on the character of the porosity. Intragranular pores typically have a near spherical shape. In the idealised case of randomly ordered spherical pores, an analytical expression for the corresponding thermal conductivity can be obtained:

$$\lambda_{SP}(P) = (1-P)^{3/2}\lambda_{TD}$$

Intergranular pores, on the other hand are highly non-spherical and their impact on thermal conductivity is strongly dependent on their shape and orientation. A lower bound for the thermal conductivity of a fuel with arbitrary, and possibly interconnected porosity has been suggested as [Nikolopoulos 1983]:

$$\lambda_P(P) > (1-P)^7\lambda_{TD}$$

Walter proposes to parametrise the porosity dependence of as fabricated pellets in terms of the measurable quantities closed and open porosity [Valter 2015]:

$$\lambda_P = (1-P_c)^a(1-P_o)^b\lambda_{TD}$$

where P_c is the fraction of closed porosity, P_o is the fraction of open porosity and the exponents a and b are determined experimentally for a given fabrication route.

Impact of radiation

Accumulation of solid fission products, gas bubble formation and radiation damage resulting from irradiation are phenomena which will influence the thermal conductivity of the fuel. The formation of gas bubbles with intrinsically low thermal conductivity can be considered as an increase in porosity of the fuel.

We therefore write the thermal conductivity as function of burn-up in the following form [Lucuta 1996]:

$$\lambda(T,B) = \kappa_{DFP}(T,B)\kappa_{PFP}(T,B)\kappa_{rad}\lambda_P(T)$$

In an oxide fuel, fission products dissolved into the matrix will reduce the conduction by phonons, while precipitating fission products will have the opposite effect. Based on lattice conduction theory and measurements of fuels with inclusions of simulated fission products, the following expression for the degradation factor related to fission products dissolved in UO_2 was suggested:

$$\kappa_{DFP}(B,T) = \left(a(B) + b(B)\sqrt{T}\right)\ arctan\left(\frac{1}{a(B)+b(B)\sqrt{T}}\right)$$
$$a(B) = \frac{1.09}{B^{3.625}}, b(B) = \frac{0.0643}{B^{0.5}}$$

where the burnup B is given in atomic percent . The impact of precipitated solid fission products is expressed in the following form:

$$\kappa_{PFP}(B,T) = 1 + \frac{0.019B}{3 - 0.019B} \frac{1}{1 + \exp\left(-\frac{T-1200}{100}\right)}$$

where the threshold at 1200 K reflects that precipitation mainly occurs in the hotter parts of the fuel.

The reduction of conductivity due to appearance of radiation damage in UO_2 is significant only at T < 1200 K, since defects anneal out at higher temperatures. The effect saturates early in fuel life and may hence be parametrised independently of burn-up as

$$\kappa_{rad} = 1 - \frac{0.2}{1 + exp\left(\frac{T-900}{80}\right)}$$

Figure 6.2 depicts the temperature dependence of the change in thermal conductivity. The dominating effect is the accumulation of fission products dissolved into the fluorite lattice. The corresponding conductivity of UOX fuel is displayed in Figure 6.3, highlighting the necessity of taking the degradation of burn-up into account. Note that this figure does not take into account the effective increase in porosity due to gas bubble formation.

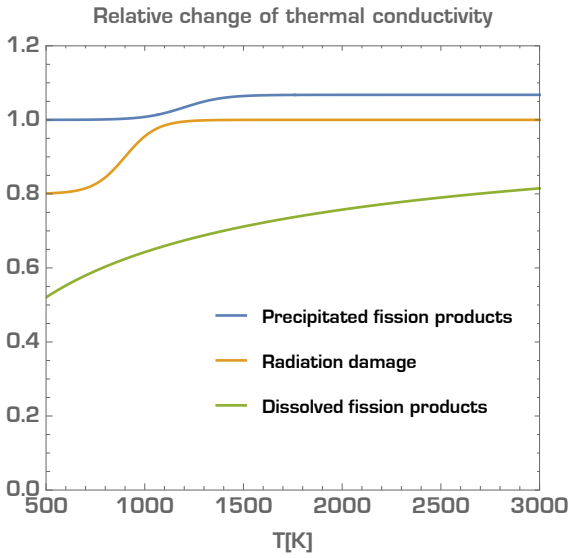

Figure 6.2: Contributions to change in thermal conductivity of UO_2 fuel [Lucuta 1996]

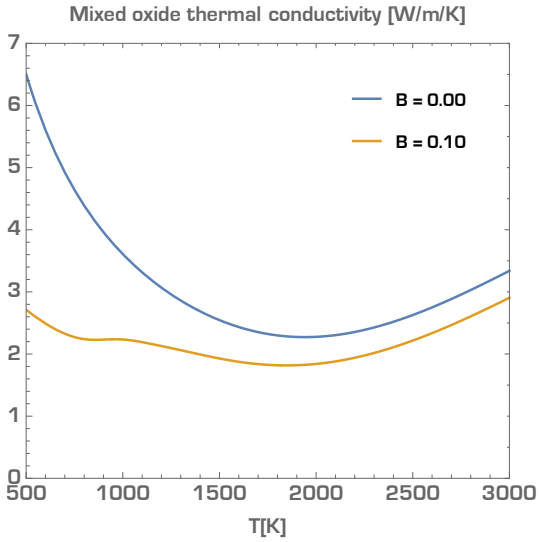

Figure 6.3: Change in thermal conductivity of UO_2 fuel [Lucuta 1996]

Metal alloy fuels

The thermal conductivities of metallic alloy, nitride and carbide fuels are much higher than for the corresponding oxides. Whereas actinide nitrides and carbides are brittle ceramics, their thermophysical properties resemble those of metals. Since the dominating contribution to thermal conductivity will come from electrons, a much larger dependency on atomic number can be expected.

The following parametrisations have been recommended for the thermal conductivity of uranium metal and for U-10Zr alloys [Touloukian 1970, Simunovic 2009]:

$$\lambda_U(T) = 21.7 + 1.59 \times 10^{-2} T + 5.91 \times 10^{-6} T^2$$

$$\lambda_{U-10Zr}(T) = 9.62 + 2.25 \times 10^{-2} T + 3.27 \times 10^{-6} T^2$$

Experimental data for the thermal conductivity of the five metallic plutonium phases were published by Los Alamos [Andrew 1981] and are displayed in Figure 6.4

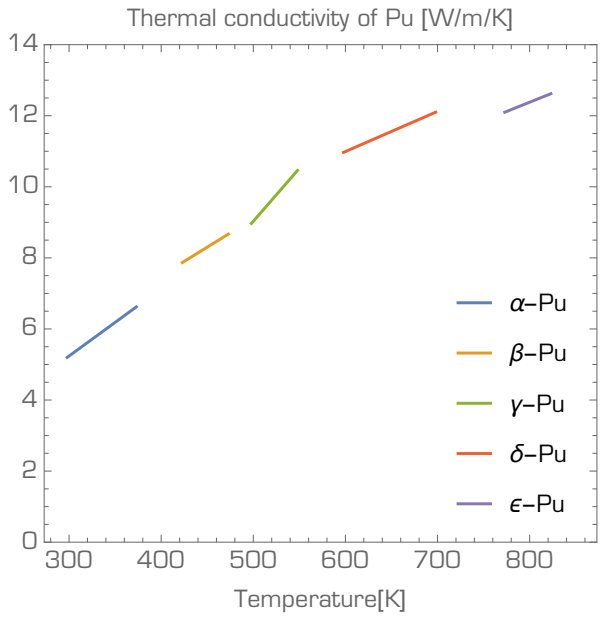

Figure 6.4: Thermal conductivity of the five metallic plutonium phases.

Argonne National Laboratory measured the thermal conductivity of U-Pu-Zr alloys [Crewe 1966]. For U-15Pu-10Zr, the data can be fitted to the following function:

$$\lambda_{U-15Pu-10Zr}(T) = -4.3 + 0.041T - 8.6 \times 10^{-6} T^2$$

The thermal conductivity of two U-20Pu-2Am-10Zr alloys was measured JAEA [Nishi 2015], the average value of which may be expressed as:

$$\lambda_{U-20Pu-2Am-10Zr}(T) = 0.67 + 0.020T + 10.0 \times 10^{-6} T^2$$

Data for for metallic americium are not available in the open literature. A theoretical estimate based on electrical resistivity is given as [Kim 2002]:

$$\lambda_{Am}(T) = 4.118 + 1.8 \times 10^{-2} T + 5.35 \times 10^{-6} T^2$$

Figure 6.5 compares the expressions for uranium metal with the alloys containing 10 wt% Zr.

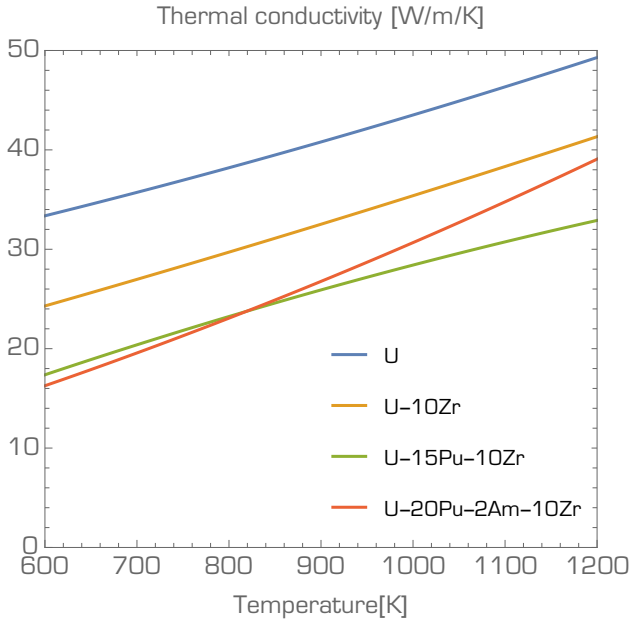

Figure 6.5: Thermal conductivity of uranium metal and metal alloy fuels.

Recall that metal alloy fuels swell rapidly under irradiation and therefore acquire 25% porosity within two percent burn-up, which will reduce the effective thermal conductivity by a factor of two.

Nitride fuels

The thermal conductivity of nitride fuels is characterised by the metallic character of their chemical bonds, leading to a conductivity increasing from room temperature up to at least 1600 K. The following functional form was suggested to represent the conductivity of UN at 100% TD [Hayes 1990]:

$$\lambda_{UN}(T) = 1.864 \times T^{0.361}$$

Measurements of PuN and AmN conductivity have been carried out in Japan [Arai 1992, Nishi 2006]. Functional forms have been fitted to these data and read as [Uno 2020]:

$$\lambda_{NpN}(T) = 7.89 + 0.0127 \times T - 4.32 \times 10^{-6} T^2$$

$$\lambda_{PuN}(T) = 8.18 + 0.0522 \times T - 9.44 \times 10^{-7} T^2$$

$$\lambda_{AmN}(T) = 8.99 + 0.00147 \times T - 2.54 \times 10^{-8} T^2$$

These are graphically displayed in Figure 6.6. One may note that as in the case of metal fuels, the conductivity of UN is considerably higher than that of PuN and AmN.

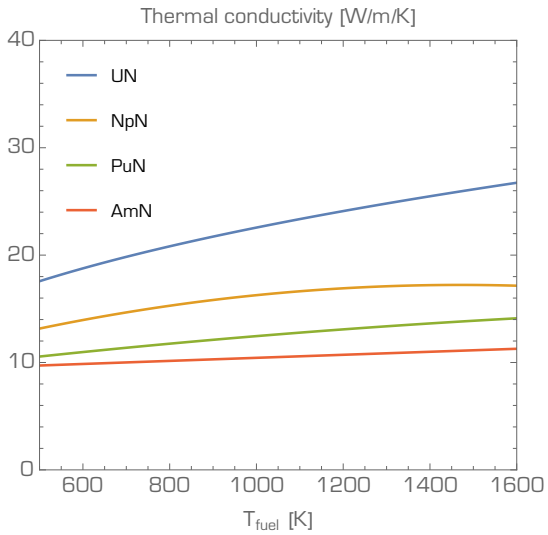

Figure 6.6: Thermal conductivity of UN, PuN and AmN, evaluated at 100% TD.

For mixed nitrides, one may approximate the thermal conductivity by a linear combination of thermal resisitivities of the pure compounds:

$$\lambda_{(U_x,Pu_y,Am_{1-x-y})N}(T) \simeq \left[\frac{x}{\lambda_{UN}(T)} + \frac{y}{\lambda_{PuN}(T)} + \frac{1-x-y}{\lambda_{AmN}(T)} \right]^{-1}.$$

Carbide fuels

The thermal conductivity of actinide carbides was measured for UC and $PuC_{0.94}$ and may be parametrised as [Connick 1975, Matzke]:

$$\lambda_{UC} = 19.5 + 3.57 \times 10^{-6} \ (T - 1123)^2$$

$$\lambda_{PuC} = 7.45 - 4.04 \times 10^{-3} T + 1.20 \times 10^{-5} T^2$$

which are plotted in Figure 6.7. For AmC, no data exist, partially because the poor high temperature stability of AmC makes it difficult to sinter pellets to any appreciable density without loss of Am.

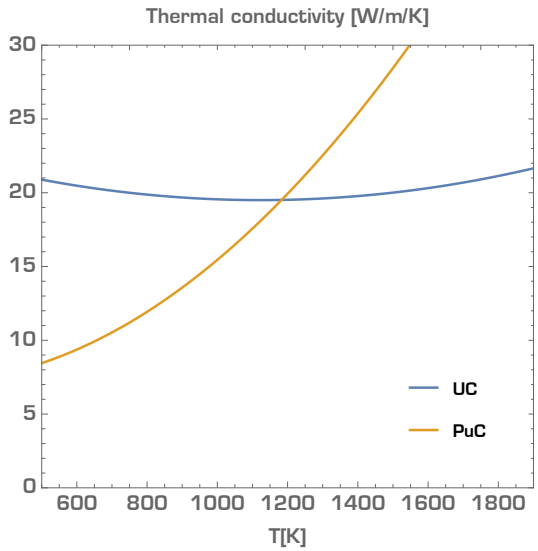

Figure 6.7: Thermal conductivity of UC and PuC.

Melting temperature

Recently measured melting temperatures of the elemental actinide dioxides are given in Table 6.1 [De Bruycker 2011, Kato 2008]. For a mixed dioxide, the solidus temperature may be taken as the concentration weighted average, corrected with a eutectic term. The latter has been estimated as $\Delta T_{melt} = -121\ C_U\ C_{Pu}$ for $(U,Pu)O_2$. The effect of sub-stoichiometry is also important, with the solidus temperature being reduced by approximately 1000 (2 - O/M) [Edwards 1990].

Table 6.1: Measured melting temperatures for actinide dioxides.

Compound	T_{melt} [K]
UO_2	3130±20
PuO_2	3017±28
AmO_2	2773±16

The high temperature phase diagram of actinide nitrides depends on nitrogen pressure. At sufficiently low pressure, AnN will dissociate into liquid metal and nitrogen, which is followed by vapourisation of these elements. This reaction can be suppressed by increasing the nitrogen pressure, and hence a melting temperature of the nitride can be measured. Table 6.2 displays observed or estimated melting temperatures [Olsson 1963, Olsson 1966, Spear 1968]. The data for PuN is based on a theoretical assessment for a nitrogen overpressure of 50 bar. Data for AmN appears to be absent in the literature.

Table 6.2: Measured and predicted melting temperatures for actinide nitrides under pressure.

Compound	T_{melt} [K]	P_{N2}[bar]
UN	3120±30	> 2.5
NpN	3100±30	> 10
PuN	3100	> 50

Melting temperatures of metal actinides and zirconium are given in Table 6.3 (webelements.com), together with the solidus/liquidus temperatures for U-15Pu-10Zr [Janney 2019].

Table 6.3: T_{melt} of actinide metals, zirconium, and solidus/liquidus temperatures for U-15Pu-10Zr.

Metal	T_{melt} [K]
U	1405
Np	910
Pu	912
Am	1449
Zr	2128
U-15Pu-10Zr	1428/1523

The high temperature phase diagrams of actinide carbides are relatively complicated. Uranium mono-carbide is stable up to its melting point at 2780 K. However, stoichiometric plutonium mono-carbide does

not exist and the stable hypo-stoichiometric compound PuC_{1-x} (where $x > 0.06$) decomposes into liquid plutonium and Pu_2C_3 at $T = 1900 \pm 30$ K.

Fuel manufacture

Manufacture of minor actinide bearing fuels for Generation IV reactors poses a particular challenge. Conventional powder pressing methods result in the formation of radio-active dust, which contaminates equipment, makes maintenance difficult and constitutes a health hazard. The intrinsic decay-heat production limits the amount of materials that can be handled without forced cooling. Poor high-temperature stability under atmospheric pressure limits the applicability of conventional sintering methods, and intense gamma and neutron activity requires complex, and therefore expensive, shielding configurations.

The end products of the PUREX process today used in reprocessing industry are powders of uranium and plutonium oxides. These powders are mixed and milled before pressing into mixed oxide pellets take place. If the same approach would be taken for fabrication of americium and curium bearing fuels, the resulting dust could constitute a major problem for dose management during maintenance and decommissioning of equipment.

Altogether, this is an incentive for abandoning "dry" powder manufacturing routes in favor of "wet" methods generating less dust, thus reducing risks for contamination.

Oxide fuels

Two wet routes for synthesis of transuranium bearing oxides have been extensively investigated: solution-gelation (sol-gel) processes relying on mixing metal nitrates with gelating agents, and co-precipitation of oxalates. Both of these methods permit the last step of the PUREX process, i.e. precipitation of oxide powders from nitric acid solutions, to be eliminated.

Co-precipitation of actinides dissolved in nitric acid, using an excess concentration of oxalates may be carried out according to [Pillon 2006, Jankowiak 2008]:

$$(Pu^{4+})_x + (Am^{3+})_{1-x} + \frac{4x + 3(1-x)}{2} C_2O_4^{2-} \rightarrow Pu_xAm_{1-x}(C_2O_4)\frac{4x + 3(1-x)}{2},$$

followed by calcination on air to form a solid solution oxide powder:

$$Pu_xAm_{1-x}(C_2O_4)\frac{4x + 3(1-x)}{2} + O_2 \rightarrow (Pu_x, Am_{1-x})O_2 + [4x + 3(1-x)]CO_2.$$

Whereas this process avoids the milling state, it still requires to manage powders during pressing. In order to eliminate this latter stage of powder management, sol-gel processes may be utilised.

The sol-gel process for manufacture of uranium oxide micro-spheres was originally developed at Oak Ridge National Laboratory [Clinton 1966]. The "internal" gelation process developed by PSI consists of mixing actinide nitrate solutions with the gelating agent $(CH_2)_6N_4$ (hexamethylene tetramine) and a stabilizer having the purpose of avoiding premature gelation. The latter agent is usually taken to be urea ($CO(NH_2)_2$) The mixture is dropped through a vibrating nozzle into silicon oil having a temperature of 380 K. Hydroxide microspheres are then formed which may be converted to oxides by thermal treatment [Ledergerber 1992]. Low density microspheres can be crushed and pressed into pellets for subsequent sintering. Alternatively one may directly fill a fuel pin with high density microspheres having three different radii, followed by vibro-packing into a so called "sphere-pac" fuel. Smear densities of up to 94% is achievable with the latter method. Dust formation can be completely avoided, although liquid wastes contaminated with americium arise.

Sintering of minor actinide bearing oxide fuels up to the desired pellet density (90-95% TD) may be achieved at a temperature below 1700°C, and is in general not a problematic issue.

Nitride fuels

Nitride powders may be synthesised from a variety of source materials. For industrial applications, it is of interest to minimise the number of process steps. Moreover, the process applied should be amenable to conservation of $^{15}N_2$ gas, if possible.

In the context of Generation-IV reactors, this means that the preferred source of depleted uranium is the UF_6 waste stream from uranium enrichment plants. This can be converted to depleted UN by ammonolysis, which entails the reaction of gaseous uranium hexafluoride with ammonia at 373-673 K, resulting in the formation of uranium ammonium fluoride complexes according to:

$$UF_6 + x\,NH_3 \rightarrow (UF_4)_3(NH_4F) + (UF_4)(NH_4F)_4 + (UF_4)_6(NH_4F)_7$$

Figure 6.8 shows a sample of uranium ammonium fluoride powder synthesized from UF_6 at KTH.

Figure 6.8: Uranium ammonium fluoride powder produced by ammonolysis of UF_6 [Zagoraios 2022].

Increasing the furnace temperature to 1073 K, keeping the reaction product under a stream of ammonia, UN_2 is formed. Finally, raising the temperature to 1400 K, UN_2 dissociates into UN and nitrogen gas:

$$2UN_2 \rightarrow 2UN + N_2$$

The entire process may be carried out in a single furnace with a liner of tantalum, that has been shown to be resistant to reaction with hydrofluoric acid (HF) at T = 1400 K [Mishchenko 2020]. The end product is theoretically free of both oxide and carbide impurities. Recovery of ^{15}N by recycle of nitrogen gas and ammonium fluoride appears to be feasible.

The synthesis of transuranium nitrides would necessarily start from the product of reprocessing, which in the case of industrially mature aqueous processing will be plutonium and americium oxides. These will be converted to nitrides by the carbo-thermic nitriding process, according to:

$$2AnO_2 + 4C + N_2 \rightarrow 2AnN + 4CO$$

Where An represents either Pu, Am or a solid solution thereof. The reaction proceeds in the temperature range of 1350° - 1550°C [Bardelle 1992, Arai 1994, Nishi 2006]. A surplus of carbon is usually added to the process, in order to ensure complete conversion of the oxide. Hence, residual carbon has to be removed during a de-carburisation step, where the initial reaction product is exposed to a stream of N_2-H_2. The reaction product in this step is mainly hydrogen cyanide (HCN) [Bardelle 1992, Jolkkonen 2004]. Inevitably, there will be residues of oxygen and/or carbon, but they may be limited to less than 1000 ppm weight each (2% of light atoms).

The process can be applied to the conversion of microspheres produced by the sol-gel method, thus avoiding dust formation [Ledergerber 1992, Hedberg 2020]. The associated gas production leads to a fairly low density of the produced microspheres.

Due to the need for continuous removal of CO and HCN, the carbo-thermic nitriding process leads to large losses of ^{15}N, and should therefore only be used for the relatively costly recycle of transuranium elements. Alternatively, natural nitrogen may be used for this purpose, as long as ^{15}N is used for the production of UN. The associated neutronic penalty and ^{14}C production would still be suppressed by a factor of 7-8.

Sintering of americium bearing nitride compounds would have to be carried out under an atmosphere of nitrogen, in order to avoid losses of americium at temperatures above 1300°C . Even under nitrogen, the sintering temperature has to be limited to 1550°C [Jolkkonen 2004]. The achievable density for nitride pellets sintered in a conventional furnace at this temperature is limited to less than 80% TD [Nishi 2006].

Hence, the only industrially viable option for producing an americium bearing driver fuel or blanket appears to be the use of spark plasma sintering (SPS) [Muta 2008, Malkki 2015, Johnson 2016]. This process entails driving a strong current (≈ 1000 A) through a powder under pressing. The current serves the dual function of providing resistance heating of the powder as well as enhancing diffusion. UN pellets with a density of 96% TD have been manufactured at a sintering temperature of 1450°C [Johnson 2016], which would allow to produce high quality nitride pellets without losses of americium. Moreover, the microstructure of the pellet can be controlled by means of suitable combinations of sintering time, temperature and pressure [Johnson 2018]. SPS may also be applied to the sintering of pellets from low density microspheres, permitting to achieve high density pellets [Hedberg 2020].

The scale-up of spark plasma sintering is limited to the current capacity of a single apparatus, which is of the order of 100 pellets per shot, requiring a peak power supply of 1 MW. Considering that the time required for ramping up temperatures, holding at peak temperature and cooling would be of the order of 15 minutes, a single SPS machine is capable of producing 10 000 pellets per day. This is roughly equivalent to 100 fuel rods, meaning that the nitride fuel for a Gen-IV fast reactor could be manufactured in a year.

It should be noted that the actual manufacture of Pu and Am bearing nitride fuels with SPS yet has to be demonstrated.

Chemical potentials

Oxide fuels

The oxygen potential $\Delta G(O_2)$ reflects the equilibrium between oxygen present in the solid crystal and the oxygen in the gas phase. It is defined from the following relation:

$$\frac{\Delta G(O_2)}{RT} = \ln\left(\frac{P(O_2,T)}{P(O_2,STP)}\right),$$

Where $P(O_2,STP)$ denotes the partial pressure of oxygen at room temperature and atmospheric pressure. The oxygen potential is a function of oxygen to metal (O/M) ratio. A positive value for a given stoichiometry means that the compound tends to loose oxygen when exposed to a gas containing 21% O_2, at atmospheric pressure and room temperature, whereas a negative value implies that an oxygen uptake will occur. Increasing the temperature makes the oxygen potential more positive and therefore reduces the equilibrium O/M ratio.

In a fuel rod, the pressure of oxygen in the bonding gas is very low at the start of irradiation. Hence, compounds with a slightly negative oxygen potential will give off oxygen until a sufficiently low O/M ratio is obtained. Moreover, this balance is affected by the build-up of fission products.

Adding minor actinides to the fuel (or blanket) has a substantial impact on the oxygen potential. Figure 6.9 compares the oxygen potential of americium oxide to that of other actinide oxides at T=1600 K, which is representative of an irradiation in a fast reactor [Guéneau2012]. In order for the americium oxide to exhibit the same stability as a plutonium oxide with O/M = 1.98, i.e. $\Delta G(O_2) < -200$ kJ/mol, an O/M ratio of less than 1.8 is required.

Therefore. minor actinide bearing oxide fuels and blankets should be manufactured with a lower O/M ratio than conventional MOX fuels. The presence of neptunium may to some extent compensate for the high oxygen potential of americium.

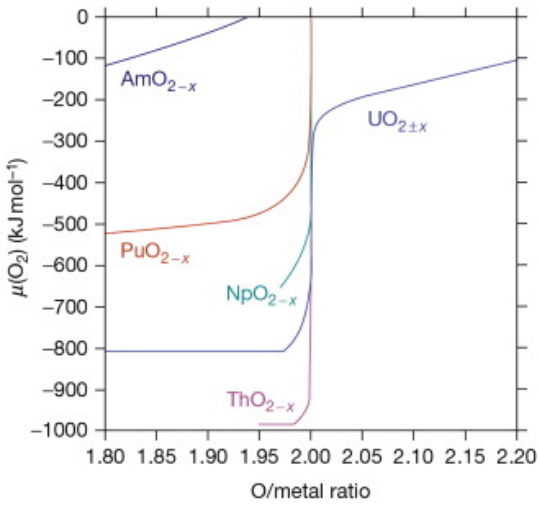

Figure 6.9: Oxygen potential as function of O/M ratio, at T = 1600 K [Guéneau 2012].

One may note that the analogue phenomenon in nitride fuels, i.e. a propensity for giving off nitrogen, is not a problem during nominal operation conditions, as the mono-nitride is the stable form of all transuranium nitrides. It does become of importance at higher temperatures, where decomposition of actinide nitrides into metal and nitrogen gas may occur.

Fission product chemistry

Nitride fuels

The chemical state of fission products has been assessed for (U,Pu)N and (U,Pu,MA)N [Arai 1994, Thetford 2003]. Up to a burn-up of 20%, zirconium, niobium, yttrium and rare earth elements are predicted to be soluble in the mono-nitride lattice. Molybdenum and technetium would form metallic precipitates. Whereas strontium is mainly found as Sr_3N_2 below T = 1470 K and as a metal above this temperature, barium is forming BaTe above T = 1070 K. Ruthenium and other platinum group metals form an inter-metallic with uranium, rather than with plutonium. At T < 1400 K, iodine is bound to caesium as CsI, which forms a gaseous species above this temperature. The main fraction of Cs is found as Cs_2Te below 1400 K, and in the gas phase above.

Fuel-clad chemical interaction

Oxide fuels

The combination of high operating temperature with a high chemical potential for oxygen in Gen-IV oxide fuels makes it likely for oxygen to be activated for reactions with Cs_2Te, a volatile compound that migrates to the interface between the fuel pellet and the cladding. Caesium chromate then forms according to the reaction:

$$Cs_2Te + Cr + 2O_2 \rightarrow Cs_2CrO_4,$$

reducing the ductility of the cladding.

An oxygen potential ΔGO_2 of -25 kJ/mol is necessary for this reaction to occur [Bailly 1999]. Moreover, tellurium may interact directly with the cladding to form metal tellurides.

Nitride fuels

Chemical interaction of nitride fuel with cladding steel is insignificant at respective operational temperatures [Bauer 1971, Arai 2006, Rogozkin 2013, Hania 2015]. Instances of corrosion attack is attributed to presence of sesquinitride in the fuel [Bauer 1971] or carbide/oxide impurities [Rogozkin 2003, Grachev 2017]. In the latter case, the following set or reactions may occur:

$$(1+y)\mathrm{MeO_2} + (1+x)\mathrm{MeC} \rightarrow \mathrm{Me}_{2+x+y}\mathrm{O}_{1+2y}\mathrm{C}_x + \mathrm{CO}$$

$$2\mathrm{CO} \rightarrow \mathrm{C} + \mathrm{CO_2}$$

The free carbon results in carburisation of the cladding with consequent embrittlement. In order to mitigate this phenomenon, it has been recommended to keep oxygen and carbon impurities in nitride fuels below 1500 ppm each [Rogozkin 2003].

Metal fuels

Once swelling has resulted in contact, rare earth fission products present in metal alloy fuels diffuse into the stainless steel cladding. The depth of corrosion attack on D9 alloys from irradiated U-19Pu-10Zr can be parametrised by the correlation [Carmack 2009]:

$$\delta = 1.7 \times 10^{11} \times (t - 158) \times e^{207/RT}$$

where t is the irradiation time in days and R = 8.314 J/mol/K is the general gas constant. From this expression, one would infer that contact between the fuel slug and the cladding is initiated after 158 days. This form of corrosion could be mitigated by the introduction of a cladding liner, albeit none of the so far tested liners have succeeded in eliminating the problem [Matthews 2017].

Gas release

Noble gas production in Generation IV reactor fuels comprise of the fission products Xe and Kr, as well as of He, deriving from alpha-decay of ^{242}Cm and ^{14}N(n,p)^{14}C reactions in nitride fuels. At lower operational temperatures ($T < 1/3\ T_{melt}$), these gas atoms remain as individual interstitial defects in the crystal lattice. With increasing temperature, diffusion leads to accumulation of gases in cavities and at grain boundaries. Once bubbles forming at grain boundaries grow large enough to interconnect to pellet or crack surfaces, the corresponding gases will be released to the fuel-clad gap and eventually to the gas plenum of the rod. This will lead to a Hoop stress on the fuel cladding that must be accounted for by designing the fuel rod with a sufficiently long plenum.

Oxide fuels

The gas release from oxide fuels increases rapidly over a certain temperature, known in the literature as the "Vitanza threshold". This threshold depends on burn-up and has been parametrized as [Vitanza 1979]:

$$T_{FGR>1\%}(UO_2) = \frac{9800}{ln(200 \times B)},$$

where the burn-up B is given in units of MWd/kg. The formula is valid up to a burn-up of 35 MWd/kg, after which the threshold decreases more rapidly [Volkov 2014].

In oxide fuels, the fraction of the pellet which remains below the Vitanza threshold will retain about 99% of the fission gases produced. Above the threshold, the release is close to 100%. Hence, the total release rate can reach 80-90% at high burn-up.

Nitride fuels

In general, the fission gas release observed in nitride fuels is lower than that of oxide fuels. This can be explained by the higher thermal conductivity, resulting in a lower operating temperature of the fuel. As long as the thermal energy of fission product gas atoms remains below the migration barrier, such gas atoms will remain dissolved in the fuel matrix, without means of migrating to grain boundaries and pellet surfaces.

The author of this text-book has proposed a semi-empirical correlation of gas release in nitride fuels as function of irradiation temperature T and fuel burn-up B [Wallenius 2022], which features calculated fission gas migration barriers as its main input [Claisse 2016]. The correlation reads as

$$R(B,T) = R_{at} + \frac{1 - R_{at}}{1 + D_{FG}\,(1-\sqrt{B})\,\exp\left[\frac{E_{mig}^{FG}}{k_B T}(1-\sqrt{B})\right]},$$

where $R_{at} = 0.7\%$ is the so called "a-thermal" release rate of gases due to recoil through the pellet surface, crack surfaces or to open porosity, i.e. pores that are inter-connected to the pellet surface. The values for fission product gas migration barrier and the associated diffusion coefficient calculated by Claisse and co-workers are $E_{mig}^{FG} = 3.0$ eV and $D_{FG} = 3.8 \times 10^{-7}$, respectively.

Figure 6.10 shows how the correlation fits gas release data from sodium bonded (U,Pu)N fuel irradiations conducted in the US [Bauer 1971, Storms 1988]. These data are better suited than data from helium bonded rods for determining a fission gas release correlation, since the pellet surface temperature is easier to predict throughout the irradiation.

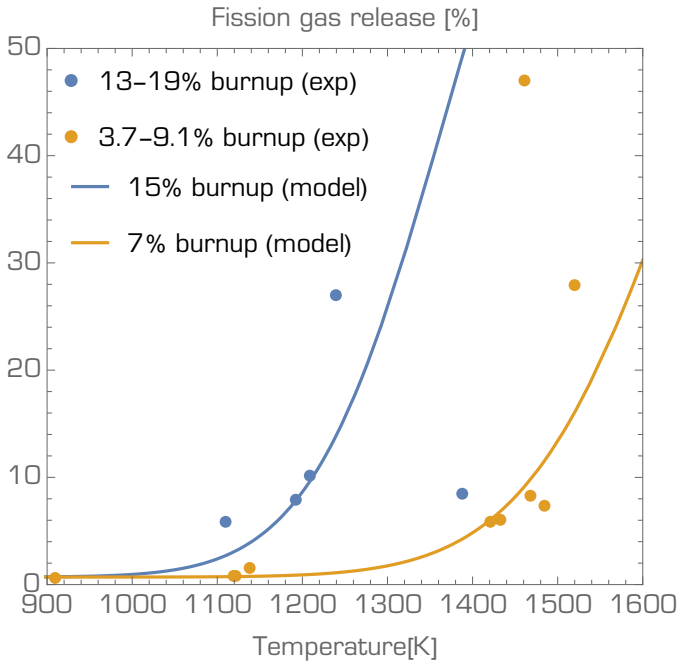

Figure 6.10: Fission gas release from sodium-bonded (U,Pu)N fuels. Circles: experimental data.

Figure 6.11 shows the predicted gas release as function of burn-up for a set of irradiation temperatures. It may be observed that for a temperature of 1200 K, gas release rates may be expected to remain on the order

of a few percent, even up to a burn-up of 10% fission in metal atoms (FIMA). At higher temperatures, the release rate may become substantial. However, it may be noted that in no irradiation of nitride fuels did the measured fission gas release exceed 50%. It is possible that even if irradiations are conducted at high linear power, the temperature in the periphery of the pellet remains below the threshold for fission gas migration, thus preventing gas release to occur in these regions.

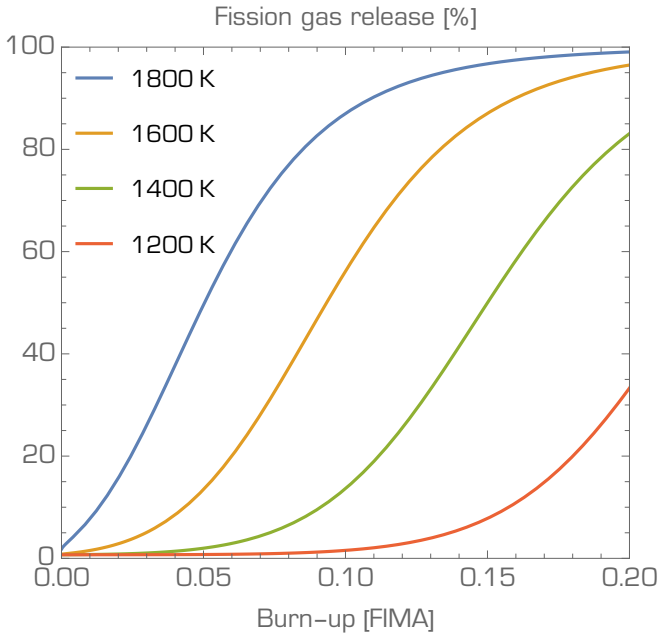

Figure 6.11: Fission gas release from nitride fuels, as predicted by the correlation of Wallenius.

Using the proposed correlation, one may calculate a Vitanza threshold for release of 1% fission gas from nitride fuels. Figure 6.12 shows the result. As may be observed, this threshold is not much different from the one derived for oxide fuels. Therefore, the main virtue of nitride fuels in this context is the lower fuel temperature that results from its higher thermal conductivity.

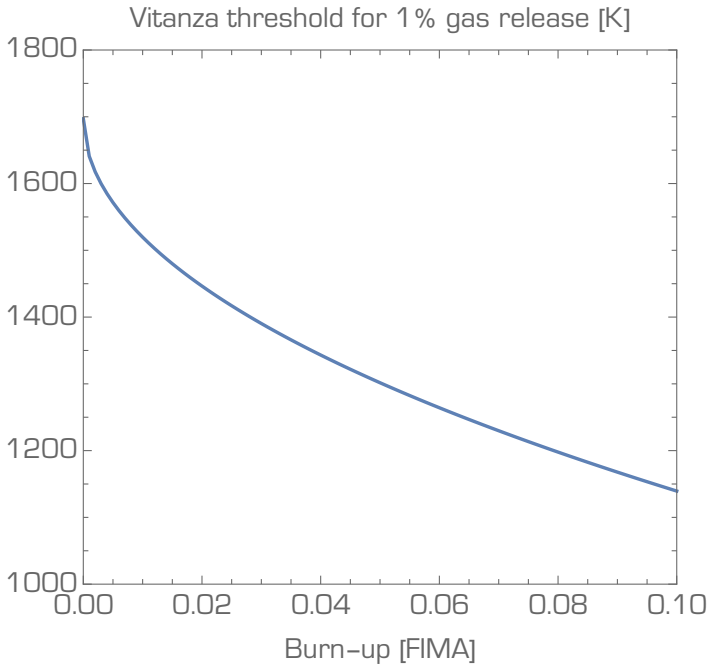

Figure 6.12: Vitanza threshold for 1% gas release from nitride fuels, obtained from the correlation of Wallenius.

Metal fuels

The fraction R of fission gas released from metal alloys fuels can be described as [Carmack 2009]:

$$R = 40 \times B, \text{ for } B \leq 0.02,$$

$$R = 0.8, \text{ for } B > 0.02,$$

where R is given in percent.

Swelling

The fission process leads to in increase of the number of atoms contained within the fuel cladding. Adopting a zeroth order approximation that fission products on average occupy the same atomic volume as actinide atoms, one would estimate a swelling rate (relative increase in volume) of the order of 0.33% per percent fission for dioxide fuels, 0.50% for mono-nitride and mono-carbide fuels and 1.0% for metallic fuels. This admittedly naïve approximation does not take into account the formation of gas bubbles, which will lead to a more rapid swelling, in particular for the denser ceramic and the metal alloy fuels

In general, one may analyze the swelling process by separately taking into account five different groups of fission products:

- Insoluble elements, forming metallic precipitates
- Insoluble elements, forming ceramic precipitates
- Soluble elements, forming a solid solution with the actinide host phase
- Volatiles
- Noble gases

The most important elements belonging to each group are listed in Table 6.4 together with their relative yields in fission of plutonium in a fast reactor with MOX fuel [Bailly 1999].

Table 6.4: Yield and chemical form of elements produced in fast neutron fission of plutonium.

Element	Fraction	Element	Fraction	Element	Fraction	Element	Fraction	Element	Fraction
Ru	0.22	Ba	0.07	Zr*	0.20	Cs	0.20	Xe	0.23
Mo	0.22	Sr	0.04	Pm	0.17	Te	0.03	Kr	0.02
Pd	0.12	Zr*		Nd	0.15	I	0.02		
Rh	0.06			Ce	0.13	Rb	0.02		
Tc	0.06			Y	0.02				
Ag	0.01								
Metal precipitates		Oxide precipitates		Soluble oxides		Volatiles		Noble gases	

*Above a certain concentration, Zr is not soluble in the MOX lattice, forming oxide precipitates.

Soluble fission products simply substitutes the fissioned actinides in their crystal lattice positions. Hence they do not have an appreciable impact on dimensional stability.

The swelling rate resulting from formation of metallic and ceramic precipitates may be calculated from the lattice parameters of the chemical compounds and is only moderately dependent on temperature.

To the noble fission products, one should add helium forming fuel to alpha-decay of actinides. At very low temperature, all noble gases remain in solution. Raising the temperature, diffusion increases and gas

bubbles form at sinks such as grain boundaries. Such bubbles will exhort a large pressure on the fuel matrix, leading to rapid swelling. Once such bubbles grow enough to interconnect with the surface of the pellet, the gas is released to the pin plenum, bringing the rapid swelling phase to a halt. The resulting gas pressure is an important design constraint for sizing of the pin plenum and will be discussed in more detail in the Chapter on core design.

Since noble gas and volatile element migration rates are highly temperature dependent, the effective swelling rate of a nuclear fuel will also be so. Therefore, predicting the actual in-pile swelling of a nuclear fuel is highly complex task, where the evolution of its thermo-mechanical and thermo-chemical state must be simulated using advanced computer codes.

Here, we will adopt a simplified approach, outlining the major trends for swelling and gas release in terms of empirical correlations. These will inform design choices that in general should be adequate, although they have to be revisited for the particular irradiation conditions of any fuel to be actually operated.

Oxide fuels

For UO_2 fuels, the solid fission product swelling rate has been calculated to be 0.32% per percent burn-up. [Anselin 1969, Spino 2005]. Observed swelling rates are higher than that, underlining the importance of gas bubble formation. In a simplistic approach, let us assume that all gas atoms created in the fuel are located in bubbles with a stable equilibrium radius r. Applying the general gas law then gives:

$$p = \frac{2\gamma}{r} = \frac{nRT}{V},$$

where $\gamma \approx 1$ J/m² is the surface energy of the oxide matrix. This leads to the following expression for the volume per gas atom:

$$\frac{V}{n} = \frac{RT}{2\gamma} r.$$

This specific volume is 2-3 times larger than the molecular volume of actinide oxides in the solid phase. The yield of xenon and krypton in fast reactor fission of plutonium is 0.25. Hence, for a burn-up of 1%, we may obtain a gas bubble with a volume being 0.50-0.75% of the solid fuel volume. Adding this increase to the one deriving from solid fission products, we find a swelling rate of 0.8-1.1% per percent of fission. Taking into account that a non-negligible fraction of the gas atoms will be dissolved in the crystal lattice of the solid, this range is compatible with swelling rates observed at low burn-up [Bailly 1999].

Once gas release into the pellet-clad gap commerces, the rate of swelling is reduced. Experimental data for MOX fuel in fast reactors are centered around an average volume increase of 0.6% per percent burn-up [Bailly 1999]. Thus, the large gas release rates observed in fast reactor oxide fuels are beneficial for reducing pellet-clad mechanical interaction.

Nitride fuels

The low gas release rate pertaining to nitride fuels means that, as compared to oxide fuels, there is a larger probability for fission gases to aggregate into bubbles that will lead to volumetric swelling of the solid pellet. Moreover, since nitride fuels are operating at a lower temperature, their creep rate is smaller, which increases the the risk of pellet-clad mechanical interaction to cause failure of the clad. Therefore, the design of a nitride fuel should ensure avoiding, or at least mitigating this interaction. To this end, it is important to understand the progress of fuel swelling as function of operational conditions.

Solid fission product swelling is unavoidable, and has been assessed at 0.5% increase in volume per percent burn-up [Arai1994]. This rate is about twice as high as that calculated for oxide fuels. Gaseous fission product swelling appears to be highly temperature dependent. Bauer states a threshold for accelerated fission gas induced swelling at 1600-1670 K [Bauer1971]. Below this threshold, the total, unrestrained

swelling rate in sodium bonded rods due to solid and gaseous fission products is given by Bauer as 1.6% per percent fission in actinides, independent of initial porosity.

A correlation for swelling in nitride fuels can be formulated based on the approach applied by Zimmerman for mixed carbides [Zimmerman 1982]:

$$\frac{\Delta V}{V} = F_1(P)\left(c_1 \times B + \left(c_2 + \frac{c_3}{1+\exp\left[-(T-T_{th})/c_4\right]}\right)\right)\left(1 - e^{-F_2(T)\times B}\right)$$

Here, F_1 characterises any dependence on as-fabricated porosity P, c_1 solid fission product swelling, c_2 and c_3 the saturated swelling rate at very high temperature, T_{th} and c_4 the threshold for accelerated gaseous fission product swelling, and F_2 the transition from fission gas dominated swelling to saturated swelling. The temperature T to be applied is reasonably the average temperature of the zone where restructuring, gas release and swelling takes place.

Figure 6.13 compares the temperature dependence of this correlation for two different burn-ups, with experimental data points from unrestricted swelling of UN and (U,Pu)N fuels. The following values for the constants in the correlation are applied: $c_1 = 0.8$, $c_2 = 10$, $c_3 = 24$, $c_4 = 80$ K, $T_{th} = 1280$ K. The functions F_1 and F_2 have been fitted by the current author as:

$$F_1(P) = e^{0.04-P},$$

$$F_2(T) = 0.08 + 1000 \times e^{-17000/T}.$$

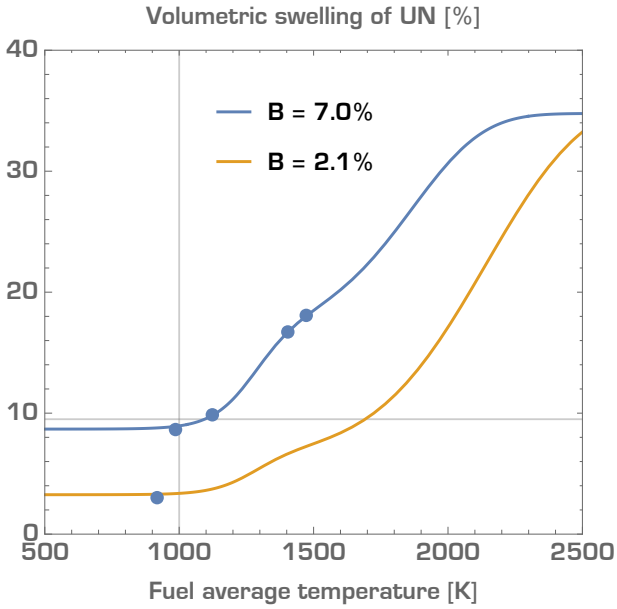

Figure 6.13: Un-restrained swelling of nitride fuels at 2% and 7% burn-up. Filled circles represent experimental data, solid lines, the here presented correlation.

One may infer that a possible approach to designing a nitride fuel rod is to ensure that the temperature of the restructuring zone remains below 1000 K for a pellet-clad gap that accommodates an increase in pellet radius of about 0.5% per percent burn-up at end-of-life. In this approach, the porosity of the fuel should be minimised, in order to reduce the operating temperature.

Another approach is to select an operating temperature above the gaseous fission product swelling threshold and design the fuel with an initial porosity large enough (≈15%) that the cladding can tolerate mechanical

interaction with the pellet. This solution has been adopted for fast reactor development in Europe [Blank 1989], Japan [Tanaka. 2004] and in Russia [Rogozkin 2011, Grachev 2017].

Yet a third approach is to design the nitride fuel with a sodium bond and a large pellet-clad gap, accommodating solid and fission gas induced swelling up to the intended burn-up. This route has been investigated mainly in the US [Bauer 1971, Hilton 2006].

Metal fuels

In liquid metal cooled reactors, metal alloy fuels feature a very large initial swelling rate, which is why they are fabricated with a large, sodium bonded fuel-clad gap. Once the fuel slug volume has increased by 30%, the generated porosity becomes interconnected, fission gas release occurs and the swelling rate is dramatically reduced. The following dependence of swelling on burn-up B has been quoted [Carmack 2009]:

$\Delta V/V = 150 \text{ x } B$, for $B \leq 0.02$,

$\Delta V/V = 0.30 + 0.5 \text{ x } B$, for $B > 0.02$.

Here, the volumetric swelling $\Delta V/V$ is given in percent.

Carbide fuels

Experimental data on swelling in carbide fuels have been parametrised by Zimmerman as

$$\frac{\Delta V}{V} = 0.8 \times B + \left(10 + \frac{24}{1 + \exp\left[-(T - 1400)/74\right]}\right)\left(1 - e^{-F_2(T)\times B}\right)$$

In the carbide case, the function describing the dependence the transition from fission gas dominated to saturated swelling is suggested as [Zimmermann 1982]:

$$F_2(T) = 0.06 + 8025 \times e^{-20270/T}.$$

Fuel-clad mechanical interaction

In sodium or lead-cooled reactors, the fuel cladding materials considered are either ferritic steels with a high threshold for irradiation induced swelling, such as HT-9, or titanium stabilised austenitic steels, such as 15-15Ti or D9.

One may parametrise the steady state thermal creep rate by the following equation:

$$\dot{\epsilon}(T) = A \times \sigma^b e^{-Q/RT},$$

where σ is the applied stress, b is the stress exponent and Q is the corresponding activation energy.

Nitride fuels

If a nitride fuel pellet is contacting the cladding, accommodation of remaining fuel swelling by creep is necessary to mitigate clad deformation and eventual failure of its barrier function. At the same temperature, the creep rate of actinide nitride fuel is much lower than that of the corresponding oxide [Rogozkin 2003]. Increasing the porosity of the nitride pellet form 5% to 15% increases the creep rate by an order of magnitude, an approach that has been taken to permit fuel-clad mechanical interaction for this type of fuel in Europe, Japan and in Russia.

Metallic fuels

Metallic fuels designed with 75% smear density reach a porosity of 30% prior to contact between the fuel slug and the cladding occurs. At this point, the creep rate of the fuel is very high and failure of the cladding due to mechanical interaction is not anticipated.

Dissolution

By definition, actinides present in spent fuel of Generation IV reactors must be possible to recover, using methods that are industrially applicable at a competitive cost. The first step in the recycling process is the dissolution of the spent fuel in an adequate medium. The solution of the spent fuel then constitutes the precursor for extraction (i.e. separation) of the actinide elements.

The medium into which the spent fuel is dissolved may be aqueous, in the case of which we speak about hydrometallurgical processing. Alternatively, molten metals or molten salts may be used for the purpose, whence we are concerned with pyrometallurgical processes. The former is the base of industrial scale reprocessing (> 100 ton/year) currently carried out in France, Russia and India. The latter has ben demonstrated on a scale of 1 ton/year in Idaho and Dimitrovgrad.

Oxide fuels

There is an established limit of about 35% Pu permitting dissolution of mixed oxide fuels without the aid of catalysts like silver or hydrofluoric acid. However, Generation IV reactor fuels with a conversation ratio above unity would feature a plutonium fraction much below that. Moreover, minor actinide oxides are soluble in nitric acid with a rate that is sufficient for industrial applications.

Nitride fuels

Fresh UN and electron irradiated $(U_{0.85},Pu_{0.15})N$ dissolves rapidly in nitric acid under conditions representative for industrial reprocessing [Sears 1970, Renard 2002]. The impact of impurities and porosity on the dissolution rate of UN pellets was shown to depend mainly on the amount of open porosity of the pellet [Aneheim 2015]. Elimination of open porosity increases the time required for dissolution by an order of magnitude.

Metallic fuels

Whereas actinide metals readily dissolve in nitric acid, the sodium bond used in liquid metal cooled fast reactor metal alloy fuel rods makes impossible to apply aqueous reprocessing. Instead, pyroprocessing (dissolution in molten metals or molten salts) is foreseen, and has been demonstrated on pilot scale (1 ton spent fuel/year) in the EBR-II spent fuel processing facility in Idaho.

Exercises:

1) Calculate the thermal conductivity and fuel temperature of MA bearing fuels
2) Calculate the oxygen potential for MA bearing oxide fuels
3) Evaluate the cost penalty for introduction of metallic/nitride fuels

Questions:

1) How does MA introduction influence thermal conductivity of fast reactor fuels?
2) How does the volatility of americium limit the manufacture of dense fuels?
3) What is the impact on gas release and fuel swelling?

References

Emma Aneheim,
Dissolution performance of unirradiated nitride fuels,
D3.1.2 of the FP7 ASGARD project, Chalmers University of Technology (2015).

F. Anselin,
USAEC Report GEAP-5583, General Electric, 1969

Y. Arai et al.,
Dependence of the thermal conductivity of (U,Pu)N on porosity and plutonium content,
Journal of Nuclear Materials **195** (1992) 37.

Yasuo Arai et al.,
Chemical forms of solid fission products in the irradiated uranium-plutonium mixed nitride fuel,
Journal of Nuclear Materials **210** (1994) 161.

Y. Arai, M. Akabori, and K. Minato,
JAEA's Activities on Nitride Fuel Research for MA Transmutation,
In 9th IEM on Actinide and Fission Product Partitioning and Transmutation, Nimes, France, 2006

Henri Bailly, Denise Ménessier and Claude Prunier,
The nuclear fuel of pressurized water reactors and fast neutron reactors,
Lavoisier Publishing, 1999.

Philippe Bardelle and Dominique Warin,
Mechanism and kinetics of the uranium-plutonium mononitride synthesis,
Journal of Nuclear Materials **188** (1992) 36.

A.A. Bauer et al.,
Mixed-nitride fuel irradiation performance,
Proc. Fast reactor fuel element technology, American Nuclear Society, 1971.

K. Bakker and R.J.M. Konings,
On the thermal conductivity of inert-matrix fuels containing americium oxide,
Journal of Nuclear Materials **254** (1998) 129.

H. Blank et al.,
Dense fuels in Europe,
Journal of Nuclear Materials **166** (1989) 95.

Juan J. Carbajo et al.,
A review of the thermophysical properties of MOX and UO_2 fuels
Journal of Nuclear Materials **299** (2001) 181.

W. J. Carmack et al.,
Metallic fuels for advanced reactors,
Journal of Nuclear Materials **392** (2009) 139.

Sam D. Clinton et al.,
Process for preparing oxide gel microspheres from sols,
United States Patent Office Patent 3290122, 1966.

Albert V. Crewe and Stephen Lawroski,
Reactor development program progress report,
ANL-7230, Argonne National Laboratory, 1966.

F. De Bruycker et al.,
The melting behavior of plutonium dioxide: a laser heating study,
Journal of Nuclear Materials **416** (2011) 166.

Christian Duriez et al.,
Thermal conductivity of hypostoichiometric low Pu content (U,Pu)O_{2-x} mixed oxide,
Journal of Nuclear Materials **277** (2000) 143

J. Edwards et al.,
Fast reactor data manual,
Fast reactor European collaboration report, 1990.

A.F. Grachev et al.,
Development of innovative fast reactor nitride fuel in Russian Federation: state-of-art,
In Proc. FR17, IAEA-CN245-062, 2017.

C. Guéneau, A.Chartier and L. Van Brutzel,
Thermodynamic and thermophysical properties of the actinide oxides,
Comprehensive Nuclear Materials, Elsevier, 2012.

P.R. Hania et al.,
Irradiation and post-irradiation examination of uranium-free nitride fuel,
Journal of Nuclear Materials **466** (2015) 597.

S.L. Hayes, J.K. Thomas and K.L. Peddicord,
Material property correlations for uranium mono nitride III. Transport properties,
Journal of Nuclear Materials **171** (1990) 289.

Marcus Hedberg,
Update on dense UN microspheres,
Proc. SAFETY meeting, 18-19th of March 2020.

Bruce A. Hilton, Douglas L. Porter and Steven L. Hayes,
Postirradiation Examination of AFCI Nitride and Oxide Transmutation Fuels at 8 at.%,
Topical Meeting on Nuclear Fuels and Structural Materials for the Next Generation Nuclear Reactors, Reno, Nevada, 4-8 June 2006.

A. Jankowiak et al.,
Preparation and characterization of $Pu_{0.5}Am_{0.5}O_{2-x}$-MgO ceramic/ceramic composites,
Nuclear Science and Engineering **160** (2008) 378.

Dawn E. Janney, Steven L. Hayes and Cynthia A. Adkins,
A critical review of the experimentally known properties of U-Pu-Zr alloys. Part 2: Thermal and Mechanical properties.
Nuclear Technology **206** (2020) 1.

Kyle Johnson et al.,
Spark plasma sintering and porosity studies of uranium nitride,
Journal of Nuclear Materials **473** (2016) 13.

Kyle Johnson and Denise Adorno Lopes,
Grain growth in uranium nitride prepared by spark plasma sintering,
Journal of Nuclear Materials **503** (2018) 75.

Mikael Jolkkonen, Marco Streit and Janne Wallenius,
Thermo-chemical modelling of uranium free nitride fuels,
Journal of Nuclear Science and Technology **41** (2004) 457.

M. Kato et al.,
Solidus and liquidus temperatures in the UO_2-PuO_2 system,
Journal of Nuclear Materials **373** (2008) 237.

Yeon Soo Kim and G.L. Hofman,
AAA fuels handbook,
Argonne National Laboratory, 2002.

G. Ledergerber, Z. Kopajtic, F. Ingold and R.W. Stratton,
Preparation of uranium nitride in the form of microspheres,
Journal of Nuclear Materials **188** (1992) 28.

S.E. Lemehov, V. Sobolev and P. Van Uffelen,
Modelling thermal conductivity and self-irradiation effects in mixed oxide fuels,
Journal of Nuclear Materials **320** (2003) 66.

P.G. Lucuta, Hj. Matzke and I.J. Hastings,
A pragmatic approach to modelling thermal conductivity of irradiated UO_2 fuel: review and recommendations,
Journal of Nuclear Materials **232** (1996) 166

Pertti Malkki et al.,
Manufacture of fully dense uranium nitride pellets using hydride derived powders with spark plasma sintering,
Journal of Nuclear Materials **452** (2014) 548.

Christopher Matthews et al.,
Fuel-cladding chemical interaction in U-Pu-Zr metallic fuels: A critical review,
Nuclear Technology **198** (2017) 231.

Yulia Mishchenko and Mikael Jolkkonen,
Direct manufacture of uranium nitride powders from uranium halogenides,
Proc. SAFETY meeting, 18-19th of March 2020.

Hiroaki Muta et al.,
Thermal and mechanical properties of uranium nitride prepared by SPS technique,
Journal of Material Science **43** (2008) 6429.

P. Nikolopoulos and G. Ondracek,
Conductivity bonds for porous nuclear fuels,
Journal of Nuclear Materials **114** (1983) 231.

Tsuyoshi Nishi et al.,
Thermal diffusivity of Americium mononitride from 373 to 1473 K,
Journal of Nuclear Materials **355** (2006) 114.

Tsuyoshi Nishi et al.,
Thermal conductivity of AmO_{2-x},
Journal of Nuclear Materials **373** (2008) 295–298

W.M. Olson and R.N.R. Mulford,
The decomposition pressure and melting point of uranium mononitride,
The Journal of Physical Chemistry **67** (1963) 952.

W.M. Olson and R.N.R. Mulford,
The melting point and decomposition pressure of neptunium mononitride,
The Journal of Physical Chemistry **70** (1966) 2932.

Sylvie Pillon and Janne Wallenius,
Oxide and nitride TRU fuels: Lessons drawn from the CONFIRM and FUTURE projects of the 5th European Framework Program,
Nuclear Science and Engineering **153** (2006) 245.

S.I. Porollo et al.,
Analysis of experimental data on gas release and swelling of UN fuel irradiated in BR-10 reactor,
In Proc. FR17, IAEA-CN245-081, Jekaterinburg, Russia, 2017.

Edouard Renard and Boris Rogozkin,
About applicability of PUREX-technology to fast breeder reactor mixed (U-Pu) monocarbide and mononitride fuels reprocessing,
Journal of Nuclear Science and Technology **39** (2002) Issue sup 3, page 753.

C. Ronchi et al.,
Thermal conductivity of uranium dioxide up to 2900 K from simultaneous measurement of the heat capacity and thermal diffusivity,
Journal of Applied Physics **85** (1999) 776.

B.D. Rogozkin, N.M. Stepennova and A.A. Proshkin,
Mono-nitride fuel for fast reactors,
Atomic Energy 95 (2003) 624.

B.D. Rogozkin et al.,
Thermochemical stability, radiation testing, fabrication and reprocessing of mononitride fuel,
Atomic Energy 95 (2003) 835.

B.D. Rogozkin et al.,
Results of mixed nitrides (45% PuN + 55% UN and 60% PuN + 40% UN) irradiation in BOR-60 reactor up to ~12% h.a.,
Technical Meeting on Design, Manufacturing and Irradiation Behaviour of Fast Reactors Fuels, 30 May-03 June 2011, IPPE, Russia.

B.D. Rogozkin et al.,
Results of irradiation of $(U_{0.55},Pu_{0.45})N$ and $(U_{0.4}Pu_{0.6})N$ fuels in BOR-60 up to 12 at.% burn-up,
Journal of Nuclear Materials **440** (2013) 445.

Mildred Bradley Sears,
Reactions of uranium carbonitrides and uranium nitride with aqueous solutions of hydrochloric, sulfuric and nitric acids,
Journal of Inorganic Nuclear Chemistry **32** (1970) 2971.

V. Sobolev,
Thermophysical properties of NpO_2, AmO_2 and CmO_2,
Journal of Nuclear Materials **389** (2009) 45

Karl E. Spear and James M. Leitnaker,
A consistent set of thermodynamic properties for plutonium mononitride,
Journal of the American Ceramic Society **51** (1968) 706.

J. Spino et al.,
Matrix swelling rate and cavity volume balance of UO_2 fuels at high burn-up,
Journal of Nuclear Materials **346** (2005) 131.

E.K. Storms,
An equation that describes fission gas release from UN reactor fuel,
Journal of Nuclear Materials **158** (1988) 119

Kosuke Tanaka et al.,
Fission gas release and swelling in uranium–plutonium mixed nitride fuels,
Journal of Nuclear Materials **327** (2004) 77.

Roger Thetford and Mike Mignanelli,
The chemistry and physics of modelling nitride fuels for transmutation,
Journal of Nuclear Materials **320** (2003) 44.

Masayoshi Uno, Tsuyoshi Nishi and Masahide Takano,
Thermodynamica and thermophysical properties of nitride fuels,
Comprehensive Nuclear Materials, 2nd edition.

Mikael Valter,
Thermal conductivity of uranium mono nitride,
MSc thesis, LITH-IFM-A-EX—15/3096—SE, Linköping University, 2015.

C. Vitanza, E. Kolstad and U. Graziani,
Fission gas release from UO_2 pellet fuel at high burnup,
Proceedings of ANS Topical Meeting on Light Water Reactor Fuel Performance, Portland, OR, 1979.

Boris Volkov et al.,
Halden fuel and material experiments beyond operational and safety limits,
Proceedings of WRFPM 2014, Sendai, Japan, Sep. 14-17, 2014

Janne Wallenius,
Transmutation of nuclear waste,
LeadCold games and books, 2011.

Janne Wallenius,
An improved correlation for gas release from nitride fuels,
Journal of Nuclear Materials **558** (2022) 153402

S.C. Weaver, J.L. Scott, R.L. Senn and B.H. Montgomery,
USAEC Report ORNL-4461, Oak Ridge National Laboratory (1969).

G. Zagoraios,
Synthesis of uranium nitride fuel from UF_4 stock,
MSc thesis, KTH, 2022.

H. Zimmermann,
Investigation of swelling of U-Pu mixed carbide,
Journal of Nuclear Materials **105** (1982) 56.